SAND2008-0298C

Numerical Examination of Two-Dimensional Smolder Structure in Polyurethane Foam

A. B. Dodd[1,2,a], C. Lautenberger[2], and A.C. Fernandez-Pello[2]

[1]Sandia National Laboratories[b], Albuquerque, NM, 87185

[2]Department of Mechanical Engineering, University of California at Berkeley, Berkeley, California, 94720

Corresponding Author:
Amanda B. Dodd
63 Hesse Hall
University of California at Berkeley
Berkeley, CA
Fax:
Email: abdodd@me.berkeley.edu

Colloquium: Fire Research

Length of Paper:
Method 1:
- Main text: 2498
- Nomenclature: 395.2
- References: 576.4
- Figure:
  - 1: 151.2
  - 2: 276.2
  - 3: 299.1
  - 4: 478.9
- Table:
  - 1. 197.6
  - 2. 152
- Equations:
  - Total: 775.3

Total: 5800

[a] Formerly A. J. Barra

[b] Sandia is a multiprogram laboratory operated by Sandia Corporation, a Lockheed Martin Company, for the United States Department of Energy's National Nuclear Security Administration under contract DE-AC04-94AL85000.

Abstract

Although smolder combustion has been extensively studied both computationally and experimentally, relatively few theoretical studies have examined the two-dimensional structure of the smolder wave. In this paper, two-dimensional smolder in polyurethane foam is modeled with a two-dimensional numerical formulation that includes a seven-step kinetic model of the polyurethane smolder reaction mechanism. The two-dimensional model formulation includes the effects of heat, mass, species, and momentum transfer of the porous solid and gas phase. The seven-step decomposition reaction mechanism, which includes a secondary char oxidation and an additional char pyrolysis step, was developed using genetic algorithm optimization. The model was used to study the two-dimensionality of a forward propagating smolder wave. The model results show a two-dimensional structure in the temperature, species, and reaction profiles that agrees qualitatively with experimental observations. Oxygen is consumed at the reaction front, as expected, which leads to different reaction pathways governing the final products (i.e. thermal char and oxidative char). It was found that the model response is sensitive to boundary conditions, thermal properties, and heats of reaction for the char oxidation reaction. The incorporation of the secondary oxidation reaction step in the model paves the way to further analysis of the transition to flaming process.

Keywords: smolder, two-dimensional, polyurethane foam, pyrolysis, microgravity

Nomenclature

Letters

A	Reactant species
c	Specific heat capacity (J/kg-K)
D	Diffusivity (m^2/s)
E	Activation energy (J/mole)

h Enthalpy (J/kg)

h_{cv} Volumetric heat transfer coefficient (W/m^3-K)

ΔH Change in enthalpy (J/kg)

$\dot{j}''_j$ Diffusive mass flux of gaseous species j (kg/m^2-s)

k Thermal conductivity (W/m-K)

K Permeability (m^2) and number of condensed-phase reactions

$\dot{m}''$ Mass flux (kg/m^2-s)

M Number of condensed-phase species

M Molecular mass (kg/mol)

n Reaction order or property exponent

N Number of gaseous species

P Pressure (Pa)

$\dot{q}''$ Conductive heat flux (W/m^2)

R Universal gas constant (J/mole-K)

T Temperature (K)

t Time (s)

x Distance (m)

X Volume fraction (-)

Y Mass fraction (-)

z Distance (m)

Z Pre-exponential factor (s^{-1})

Greek symbols

γ Parameter in radiative thermal conductivity expression

ε Emissivity (-)

ν Viscosity (m^2/s) and mass fraction coefficients

ρ Density (kg/m^3)

σ Stefan-Boltzmann constant ($W/m^2\text{-}K^4$)

ψ Porosity (-)

Subscripts

A Species A

d Destruction

f Formation

g Gaseous or gas-phase

i Condensed-phase species i

j Gaseous species j

k Heterogeneous reaction k

r Reference (as in T_r) or radiative (as in k_r)

s Solid-phase (really, condensed-phase)

0 Initial (as in T_0)

∞ Ambient

Σ Integrated (summation)

Superscripts

$\bar{(\ )}$ Weighted, or averaged

1. Introduction

Smolder combustion has received considerable attention in the literature both experimentally [1]-[12] and computationally [13]-[30]. Experimental focus has ranged from studying smolder propagation to examining transition to flaming for various fuels. Most smolder combustion models presently available in literature are one-dimensional [13]-[23], with the exception of a handful of two-dimensional models [24]-[28], as well as a three-dimensional model by Saidi *et al.* [29]. Despite the widespread prevalence of polyurethane in the built environment, only one model of multi-dimensional smolder in polyurethane foam has been presented [27]. Thus, our computational understanding of multi-dimensional smolder propagation, particularly in polyurethane foam, remains limited. The present paper examines two-dimensional smolder wave propagation in polyurethane using a comprehensive numerical model. The contribution of the present work lies in the complexity of the reaction mechanism and in the two-dimensional structure of the reaction front in polyurethane. The reaction mechanism includes three pyrolysis reactions and four oxidation reactions. One of the oxidation reactions included is what has been referred to as “secondary char oxidation”, which has been identified as the key step leading to transition to flaming [10], [12]. While the current focus is not to examine the transition from smoldering to flaming, the work establishes the framework to potentially do so in the future.

2. Model Formulation

The computational model formulation includes the two-dimensional conservation equations for a thermal and oxidative reacting porous material. The equations are solved numerically using a finite difference formulation that was also utilized in previous work by Lautenberger [30]. A "zero-dimensional" transient formulation can be invoked to simulate "lumped" system with negligible gradients of temperature and species, as occurs in ideal TGA experiments. The code can also simulate both one-dimensional and two-dimensional systems. Below, the governing equations are presented for

the 2D formulation. The 2D simulations are run with a 1 mm × 1 mm grid size and a time step of 0.1 s. Reducing the grid spacing and time step by a factor of 2 resulted in no significant difference in the calculated results, so these calculations are considered sufficiently resolved.

2.1 Two-Dimensional Governing Equations

Assumptions inherent in the model formulation include:

- Each condensed-phase species has well-defined "properties": bulk density, specific heat capacity, effective thermal conductivity, permeability, porosity
- Specific heat capacity and effective thermal conductivity vary by a three-parameter model as $\phi(T) = \phi_0 (T/T_r)^{n_\phi}$ where T_r is a reference temperature, ϕ_0 is the value of k or c at T_r, and n_ϕ specifies whether ϕ increases or decreases with T
- Radiation heat transfer across pores is accounted for by adding a contribution to the effective thermal conductivity that varies as γT^3 where γ is a fitting parameter
- Averaged properties in conservation equations are calculated by appropriate mass or volume fraction weighting
- All gaseous species have equal diffusion coefficients
- Darcian pressure-driven flow through porous media
- Unit Schmidt number ($\nu = D$)
- Gas-phase and condensed-phase are in thermal equilibrium ($T=T_g$)
- There is no net shrinkage (volume change) due to reactions
- No homogeneous gas-phase reactions occur

The two-dimensional conservation equations, derived for the two-dimensional computational domain shown in Fig. 1, are presented below as Equations (1)-(8).

Condensed-phase mass conservation:

$$\frac{\partial \bar{\rho}}{\partial t} = -\dot{\omega}'''_{fg} \tag{1}$$

Condensed-phase species conservation:

$$\frac{\partial \left(\bar{\rho} Y_i\right)}{\partial t} = \dot{\omega}'''_{fi} - \dot{\omega}'''_{di} \tag{2}$$

Gas-phase mass conservation:

$$\frac{\partial \left(\rho_g \bar{\psi}\right)}{\partial t} + \frac{\partial \dot{m}''_x}{\partial x} + \frac{\partial \dot{m}''_z}{\partial z} = \dot{\omega}'''_{fg} \tag{3}$$

Gas-phase species conservation:

$$\frac{\partial \left(\rho_g \bar{\psi} Y_j\right)}{\partial t} + \frac{\partial \left(\dot{m}''_x Y_j\right)}{\partial x} + \frac{\partial \left(\dot{m}''_z Y_j\right)}{\partial z} = -\frac{\partial \dot{j}''_{j,x}}{\partial x} - \frac{\partial \dot{j}''_{j,z}}{\partial z} + \dot{\omega}'''_{fj} - \dot{\omega}'''_{dj} \tag{4}$$

$$\dot{j}''_{j,x} = -\bar{\psi}\rho_g D \frac{\partial Y_j}{\partial x} \qquad \dot{j}''_{j,z} = -\bar{\psi}\rho_g D \frac{\partial Y_j}{\partial z} \tag{5}$$

Condensed-phase energy conservation:

$$\frac{\partial \left(\bar{\rho}\bar{h}\right)}{\partial t} + \frac{\partial \left(\dot{m}''_x h_g\right)}{\partial x} + \frac{\partial \left(\dot{m}''_z h_g\right)}{\partial z} = -\frac{\partial \dot{q}''_x}{\partial x} - \frac{\partial \dot{q}''_z}{\partial z} + \sum_{k=1}^{K} \dot{Q}'''_{s,k} + \sum_{i=1}^{M} \left(\dot{\omega}'''_{fi} - \dot{\omega}'''_{di}\right) h_i \tag{6}$$

$$\dot{q}''_x = -\bar{k}\frac{\partial T}{\partial x} \qquad \dot{q}''_z = -\bar{k}\frac{\partial T}{\partial z} \tag{7}$$

Pressure evolution equation:

$$\frac{\partial}{\partial t}\left(\frac{P\bar{M}\bar{\psi}}{RT_g}\right) = \frac{\partial}{\partial x}\left(\frac{\bar{K}}{\nu}\frac{\partial P}{\partial x}\right) + \frac{\partial}{\partial z}\left(\frac{\bar{K}}{\nu}\frac{\partial P}{\partial z}\right) + \dot{\omega}'''_{fg} \tag{8}$$

Refer to the nomenclature section for explanation of all symbols. Note that a subscript *i* refers to the condensed-phase and a subscript j refers to the gas-phase. An overbar denotes a weighted or averaged quantity, i.e. $\bar{k} = \sum X_i k_i$. See [30] for details.

The governing equations described above yield a system of coupled algebraic equations that are solved numerically. The recommendations of Patankar [31] are followed closely. Due to the nonlinearity introduced by the source terms and temperature-dependent thermophysical properties, a fully-implicit formulation is adopted for solution of all equations. The gas phase species, gas phase momentum, and condensed phase energy conservation equations are solved using a computationally efficient tridiagonal matrix algorithm (TDMA). The two-dimensionality of the governing equations is handled using a line-by-line TDMA. The condensed phase mass and condensed phase species conservation equations are solved with a customized fully implicit solver that uses overrelaxation to prevent divergence. Source terms are split into positive and negative components to ensure physically realistic results and prevent negative mass fractions or densities from occurring [31]. Newton iteration is used to extract the temperature from the weighted enthalpy and the condensed phase species mass fractions. Convective terms are fully upwinded. Additional details are given in [30].

2.2 Source Terms

The governing equations presented earlier contain several source terms attributed to chemical reactions ($\dot{\omega}'''_{fi}, \dot{\omega}'''_{di}, \dot{\omega}'''_{fj}, \dot{\omega}'''_{di}, \dot{\omega}'''_{fg}$, and $\dot{Q}'''_{s,k}$) that must be quantified. Heterogeneous reaction stoichiometry is written in general form as:

$$1 \text{ kg } A_k + \sum_{j=1}^{N} \nu'_{j,k} \text{ kg gas } j \rightarrow \nu_{B,k} \text{ kg } B_k + \sum_{j=1}^{N} \nu''_{j,k} \text{ kg gas } j \qquad \text{where } \nu_{B,k} = \frac{\rho_{B_k}}{\rho_{A_k}} \tag{9}$$

Each reaction k converts a condensed-phase species having index A_k to a condensed-phase species having index B_k. Gases may be consumed or produced in the process. The destruction rate of condensed-phase species A_k by reaction k is calculated as either thermal or oxidative pyrolysis:

$$\dot{\omega}'''_{dA_k} = \left(\frac{\bar{\rho} Y_{A_k}}{\left(\bar{\rho} Y_{A_k} \right)_\Sigma} \right)^{n_k} \left(\bar{\rho} Y_{A_k} \right)_\Sigma Z_k \exp\left(-\frac{E_k}{RT} \right) \quad (\text{for } n_{O_2,k} = 0) \tag{10}$$

$$\dot{\omega}'''_{dA_k} = \left(\frac{\bar{\rho} Y_{A_k}}{\left(\bar{\rho} Y_{A_k} \right)_\Sigma} \right)^{n_k} \left(\bar{\rho} Y_{A_k} \right)_\Sigma \left[\left(1 + Y_{O_2} \right)^{n_{O_2,k}} - 1 \right] Z_k \exp\left(-\frac{E_k}{RT} \right) \quad (\text{for } n_{O_2,k} \neq 0) \tag{11}$$

$$\left(\bar{\rho} Y_i \right)_\Sigma \equiv \left(\bar{\rho} Y_i \right)\Big|_{t=0} + \int_0^t \dot{\omega}'''_{fi}(\tau)\, d\tau \tag{12}$$

The formation rate of condensed-phase species B_k by reaction k is related to condensed-phase bulk density ratios as:

$$\dot{\omega}'''_{fB_k} = \nu_{B,k} \dot{\omega}'''_{dA_k} = \frac{\rho_{B_k}}{\rho_{A_k}} \dot{\omega}'''_{dA_k} \tag{13}$$

The formation rate of all gases (conversion rate of condensed-phase mass to gas-phase mass) by reaction k is:

$$\dot{\omega}'''_{fg_k} = \left(1 - \nu_{B,k} \right) \dot{\omega}'''_{dA_k} = \left(1 - \frac{\rho_{B_k}}{\rho_{A_k}} \right) \dot{\omega}'''_{dA_k} \tag{14}$$

The net generation rate of gaseous species j from condensed phase reaction k is calculated as:

$$\dot{\omega}'''_{s,j,k} = \dot{\omega}'''_{fg_k} y_{s,j,k} \tag{15}$$

where $y_{s,j,k}$ is the N by K species yield matrix, see [30] for details.

Associated with each reaction k is a heat of reaction:

$$\dot{Q}'''_{s,k} = -\dot{\omega}'''_{dA_k} \Delta H_k \tag{16}$$

The total source terms appearing in the conservation equations are obtained by summing over all reactions: $\dot{\omega}'''_{fg} = \sum_{k=1}^{K} \dot{\omega}'''_{fg,k}$.

2.3 Reaction Mechanism

The postulated reaction mechanism used here includes seven steps:

$$\begin{aligned}
&\textit{Reaction 1:} && Foam \rightarrow \nu_{\beta,1}\ \beta - foam + \nu_{P,1}\ Thermal\ Pyrolysate \\
&\textit{Reaction 2:} && \beta - foam \rightarrow \nu_{TC,2}\ Thermal\ Char + \nu_{P,2}\ Thermal\ Pyrolysate \\
&\textit{Reaction 3:} && Thermal\ Char \rightarrow Thermal\ Pyrolysate \\
&\textit{Reaction 4:} && Foam\ +\ \nu_{O,4}\ O_2 \rightarrow \nu_{C,4}\ Char + \nu_{P,4}\ Oxidative\ Pyrolysate \\
&\textit{Reaction 5:} && Foam\ +\ \nu_{O,5}\ O_2 \rightarrow \nu_{\beta,5}\ \beta - foam + \nu_{P,5}\ Oxidative\ Pyrolysate \\
&\textit{Reaction 6:} && Char\ +\ \nu_{O,6}\ O_2 \rightarrow \nu_{\alpha,6}\ \alpha\text{-}char + \nu_{P,6}\ Oxidative\ Pyrolysate \\
&\textit{Reaction 7:} && \alpha\text{-}char\ +\ \nu_{O,7}\ O_2 \rightarrow \left(1 - \nu_{O,7}\right)\ Products
\end{aligned} \tag{17}$$

The mechanism in Equation (17) is an extension of that presented by Rein *et al.* [20], [22]. The primary difference is that two additional reaction steps corresponding to char degradation (reactions 3 and 7) are included. The mechanism consists of the following reactions: two foam pyrolysis steps (reactions 1 and 2), a char pyrolysis step (reaction 3), two foam oxidation steps (reaction 4 and 5), and two char oxidation steps (reactions 6 and 7). The subscripts *β, P, TC, α,* and *Pr* are used to represent *β*-foam, pyrolysate, thermal char, α-char, and products, respectively. The indices 1 through 7 are used to represent each reaction step as numbered in Equation (17). To simplify the model, the gaseous species "thermal pyrolysate", "oxidative pyrolysate", and "products" are tracked as a single species designated "pyrolysate" and are referred to hereafter as pyrolysate.

The 25 unknown kinetics parameters (pre-exponential factors, activation energies, reaction orders, and stoichiometry coefficients) contained in the above decomposition model were estimated from TGA data [3] in nitrogen and air environments at 20 ºC/min heating rate by genetic algorithm optimization [30]. The best-fit Arrhenius parameters are summarized in Table 1. In the oxidative pyrolysis reactions, n_{O2} was set to 1.

3. Two-Dimensional Simulation of Smolder Structure

The experiments simulated here [6] involve the forward propagation of a smolder wave through a polyurethane foam cylinder 12 cm in diameter and 14 cm in length. The experiments were conducted in microgravity on the NASA Space Shuttle (mission STS–108). Temperatures were measured with centerline thermocouples installed at eight axial locations. The sample holder was a Vespel® cylindrical shell. The smolder reaction was initiated with a porous igniter at one end of the cylinder. Air was forced into the foam sample at the igniter end so that the smolder wave propagated in the same direction as the airflow. While the igniter was energized (during the first 400 s of the experiment), the forced airflow velocity was approximately 0.01 mm/s. The igniter was de–energized at 400 s, at which time the airflow was increased to its nominal value of 5 mm/s. The Vespel sample holder acted as a heat sink, and post-test pictures indicated a two-dimensional smolder front. Thus, these experiments serve as a good qualitative test of the present 2D model. It should be noted that the experiments had an axisymmetric cylindrical geometry. However, as a first approximation to modeling two-dimensional effects, the experiment is simulated here using Cartesian (rectangular) coordinates because the primary goal of the present paper is to qualitatively examine two-dimensional smolder structure.

The computational domain is presented in Fig. 1. Convective boundary conditions are imposed on the condensed-phase energy equation at the top and sides of the domain. The temperature at the igniter (inlet) is specified to match that recorded experimentally. For the gas-phase species conservation

equation, the incoming flow composition is specified, and high Peclet number is assumed at the outlet so no boundary condition is required [31]. The sides are impermeable to mass transfer, so a zero gradient boundary condition is applied to the gaseous species conservation equations. Similarly, for the pressure evolution equation, a zero gradient boundary condition is set at the side walls to ensure a zero flux condition. At the inlet, the pressure gradient is set to give the specified mass flow rate, and the pressure at the outlet boundary is assumed to be atmospheric.

Model input parameters used in the simulations are shown in Table 1 (reaction parameters) and Table 2 (thermophysical properties). These were estimated utilizing genetic algorithm optimization. Heats of reaction and the ν coefficient for oxygen were estimated by comparing model calculations of centerline temperature to experimental thermocouple measurements. Thermal properties were estimated in a similar way using the values from Rein *et al.* [22] as a starting point.

Figure 2 shows simulation progress at 635 s, corresponding approximately to the time at which the igniter has reached its peak temperature. The temperature profile shown in Fig. 2a demonstrates the two-dimensional nature of the smolder wave. The temperature gradients are a balance between the smolder front heat release and heat losses through the boundaries. The progression of reaction 1 is shown in Fig. 2b and it can be seen that the reaction rate drops to zero at a location where the temperature profile changes from a high to a low temperature. The reaction zone thickness for reaction 1 is fairly small; this implies that as soon as reaction 1 begins the rest of the reactions progress quickly. In examining the mass fractions of species present, different reaction pathways can also be examined. The domain above the reaction front shown in Fig. 2b is pure foam and the domain below the reaction front has been consumed to form β-foam or char. Foam can be consumed through pyrolysis to form β-foam or through oxidation to form char. In examining which reaction is consuming the foam, it is found that the reaction pathways are approximately a 50/50 split. There is 50% char and 50% thermal char left in the area

upstream of the reaction front. The α-char is more prevalent near the 14 cm boundary (bottom); this is expected because fresh oxidizer flows in at this surface. Oxidizer is consumed at the reaction front, so the region directly behind the reaction front is oxygen deficient, which causes products that are formed in the absence of oxygen to form. However, at the inlet, fresh oxidizer is introduced and oxidative pyrolysis can occur. Two dimensional effects are strongly evident in the simulation. At the edges of the domain, the reaction front is quenched due to heat losses (two-dimensional effect). The reaction front propagates fasted along the centerline, where it is well insulated from the surroundings.

Figure 3a shows a post-test cross section of the foam sample and the foam mass fraction computed at the end of the simulation (Fig. 3b). The model compares qualitatively well with experimental results. From the results presented in Fig. 2 and 3, the model shows two-dimensionalities in the smolder front, which are also evident in the experimental photograph. From the above results, it is clear that the model is capable of correctly modeling two-dimensional effects of polyurethane foam. Gradients in species, temperature, reaction rates, and velocities are being appropriately captured by the model. As a result, the model will be utilized in the future to perform more complex two-dimensional calculations for a range of experimental conditions.

Figure 4 compares model and experimental temperature data. The figure shows temperature vs. time profiles at centerline thermocouple locations. Peak temperatures indicate when the smolder front passes a given location. The model portrays all of the physical processes that are present in the experimental data, except the increase and plateau seen clearly at the 2.5 and 4.5 cm locations at ~72 ºC, which is most likely water evaporation. Peak temperatures match well, smolder velocities match fairly well also. The smolder velocity calculated using experimental data is 3.3 mm/s and using model data is 2.4 mm/s. It was found that the model was not sensitive to the heat of reaction for reactions 3 and 7, the final pyrolysis step, and the final char oxidation step. This is not surprising because these two reactions play a

small role in the smolder decomposition process under the present experimental conditions. The model was most sensitive to the heat of reaction for reaction 6, the char oxidation step. This is anticipated because this reaction has been shown to be the primary source of heat release in forward smolder propagation.

In examination of the experimental data, the experimental temperature profiles start to decrease at 830 s at 2.5 cm (from the top end); this suggests that smolder reactions are no longer generating heat. The model shows that the peak temperature at 2.5 cm is at about 930 s. It is not surprising that the time to reach a peak temperature is slightly off from the experimental data because the predicted smolder velocity is slower than that in the experiment. Predicted peak temperatures are very similar to that of the experiment. In experiments, peak thermocouple temperatures ranged from 410-450 ºC. In the model, peak temperatures in the reaction zone are approximately 430 ºC.

4. Concluding Remarks

A two-dimensional computational formulation and a seven-step kinetic model were implemented to examine the two-dimensional smolder structure in polyurethane foam. Experimental results were utilized to assess the ability of the model to correctly predict two-dimensional smolder structure. The model compares very well qualitatively with experimental data. Much insight is gained through examination of the smolder propagation in two-dimensions. The inclusion of secondary oxidation reactions adds further insight regarding the reaction mechanism taking place during forward smolder propagation, in terms of reaction pathways and the effect of the presence of oxygen. Examining reaction progress, mass fraction profiles, and temperature contours aids in further understanding of important variables to the propagation of the smolder front. Simulation results are sensitive to thermal properties and boundary conditions, and care should be taken when modeling smolder propagation.

Acknowledgments

The research at UCB was supported by the National Aeronautics and Space Administration, under grants NAG3-2026, NNC-05GA02G, and NNC-04HA08H. In addition, the authors would like to acknowledge Dr. D. Urban for his support to this work, the comments of Dr. G. Rein, and Dr. C. Chao for providing the TGA data in electronic form.

References

[1] J.L. Torrero, A.C. Fernandez-Pello, Fire Safety Journal 24 (1995) 35-52.

[2] S.D. Tse, A.C. Fernandez-Pello, K. Miyasaka, Proc. Combust. Inst. 1 (1996) 1505-1513.

[3] C.Y.H., Chao, J.H.Wang , J. Fire Sci. 19 (2001) 137–156.

[4] J.H., Wang , C.Y.H. Chao, W. Kong, J. Fire Sci. 20 (2) (2002) 113-131.

[5] A. Bar-Ilan, , G. Rein, D.C. Walther, A.C. Fernandez-Pello, J.L.Torero, D.L. Urban, Combust. Sci. Tech. 176 (2004) 2027–2055.

[6] A. Bar-Ilan, G. Rein, A.C. Fernandez-Pello, J.L. Torero, D.L. Urban, Exp. Thermal Fluid Sci. 28 (2004) 743–751.

[7] T. J. Ohlemiller, Combust. Flame 81 (3-4) (1990) 354-365.

[8] C.Y.H. Chao, J.H. Wang., Combust. Flame (127) (4) (2001) 2252-2264.

[9] T. Kashiwagi, K.B. McGrattan, S.L. Olson, O. Fujita, M. Kikuchi, K. Ito, Proc. Combust. Inst. 1 (1996) 1345-1352.

[10] A. Bar-Ilan, O. Putzeys, G. Rein, A.C. Fernandez-Pello, D.L. Urban, Proc. Combust. Inst. 30, (2005) 2295-2302.

[11] C. Lu, C., J. Zhou, L. Zhang, L. Peng, Q. Lin, Q. Wang, Combust. Sci. Tech. 11, (3) (2005) 268-272.

[12] O. Putzeys, A. Bar-Ilan, G. Rein, A.C. Fernandez-Pello, D.L. Urban, Proc. Combust. Inst. 31,

(2007) 2669-2676.

[13] T. J. Ohlemiller, Progress Energy Combust. Sci, 11 (4) (1985) 277-310.

[14] S. S. Dosanjh, P.J. Pagni, A.C. Fernandez-Pello, Combust. Flame 68 (2) (1987) 131-142.

[15] D. A. Schult, B.J. Matkowsky, V.A., Volpert, A.C. Fernandez-Pello, Combust. Flame 101 (4) (1995) 471-490.

[16] D.A. Schult, B.J. Matkowsky, V.A., Volpert, A.C. Fernandez-Pello, Combust. Flame 104 (1-2) (1996) 1-26.

[17] J. Buckmaster, D. Lozinski, Combust. Flame 104 (3) (1996) 300-310.

[18] S.V. Leach, G. Rein, J.L. Ellzey, O.A. Ezekoye, J.L. Torero, Combust. Flame 120 (3) (2000) 346-358.

[19] F. De Souza Costa, D. Sandberg, Combust. Flame 139 (3) (2004) 227-238.

[20] G. Rein, A. Bar-Ilan, A.C. Fernandez-Pello, J.L. Ellzey, J.L., Torero, D.L. Urban, Proc. Combust. Inst. 30 (2) (2005) 2327-2334.

[21] G. Rein, C. Lautenberger, A.C. Fernandez-Pello, J.L. Torero, D.L. Urban, Combust. Flame 146 (1-2) (2006) 95-108.

[22] G. Rein, A.C. Fernandez-Pello, D.L. Urban, Proc. Combust. Inst. 31 (2), (2007) 2677-2684.

[23] E. M. Kallmann, *Numerical Modeling of Microgravity Smoldering Combustion in Flexible Polyurethane Foam,* PhD thesis, University of California at Berkeley, Berkeley, CA, 2005.

[24] M. K. Moallemi, H. Zhang, S. Kumar, Combust. Flame (95) (1-2) (1993) 170-182.

[25] A. Rostami, J. Murthy, M. Hajaligol, J. Analytical Applied Pyrolysis 66 (1) (2003) 281-301.

[26] C. Di Blasi, Combus. Sci. Tech. 106 (1995) 103-124.

[27] C. Ghabi, G. Rein, H.B. Ticha, M., Sassi, Progress in Computational Heat and Mass Transfer (Proceedings of the 4th ICCHMT, Paris), Vol. 1, (2005) 572-578.

[28] Z. Lu, J. Buckmaster, M. Chen, L. Massa, Combust. Theory Modeling 10 (3) (2006) 515-534.

[29] M.S. Saidi, M.R. Hajaligol, A. Mhaisekar, M. Subbiah, Applied Mathematical Modeling 31 (2007) 1970–1996.

[30] C. Lautenberger, *A Generalized Pyrolysis Model for Combustible Solids*, PhD thesis, , University of California at Berkeley, Berkeley, CA, 2007.

[31] S.V. Patankar, Numerical Heat Transfer and Fluid Flow, Hemisphere Publishing Corporation, New York, 1980.

Table 1

Reaction parameters used in calculations

Reaction	Pre-exponential Factor ($log_{10}(1/s)$)	Activation Energy (kJ/mol)	Reaction Order (-)	Heat of Reaction	ν_O (-)
1	18.5	227	0.80	40 J/g-foam	0
2	10.1	147	1.25	750 J/g-βfoam	0
3	8.9	173	0.92	-2500 J/g-thermalchar	0
4	15.1	188	0.50	-1500 J/g-foam	0.3
5	16.0	200	0.50	-1600 J/g-βfoam	0.4
6	15.0	20	0.90	-2500 J/g-char	1.5
7	8.6	153	1.61	-2500 J/g-αchar	1.5

Table 2

Condensed phase thermophysical properties

i	Name	k_0 (W/m–K)	n_k (–)	ρ_0 (kg/m^3)	N_ρ (–)	c_0 (J/kg–K)	n_c (–)	γ (m)	K (m^2)	ψ (m^3/m^3)
1	**Foam**	0.05	1.6	26.5	0	1760	0.7	0.001	5.2×10^{-9}	0.970
2	**β-foam**	0.05	1.6	18.0	0	1760	0.7	0.001	1.0×10^{-8}	0.979
3	**Thermal Char**	0.05	1.6	1.1	0	1760	0.7	0.001	3.0×10^{-8}	0.998
4	**Char**	0.05	1.6	10.0	0	1760	0.7	0.001	3.0×10^{-8}	0.989
5	**α-char**	0.05	1.6	2.4	0	1760	0.7	0.001	3.0×10^{-8}	0.997

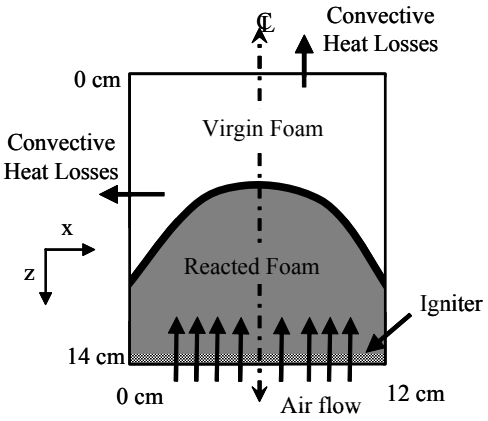

Fig. 1. Two-dimensional computational domain.

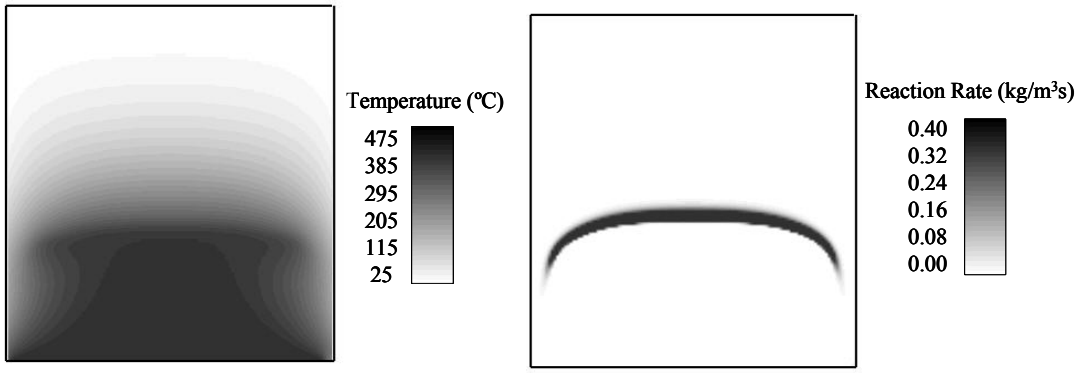

(a) **(b)**

Fig. 2. Temperature (a) and Reaction 1 reaction rate (b) contours at t = 635s.

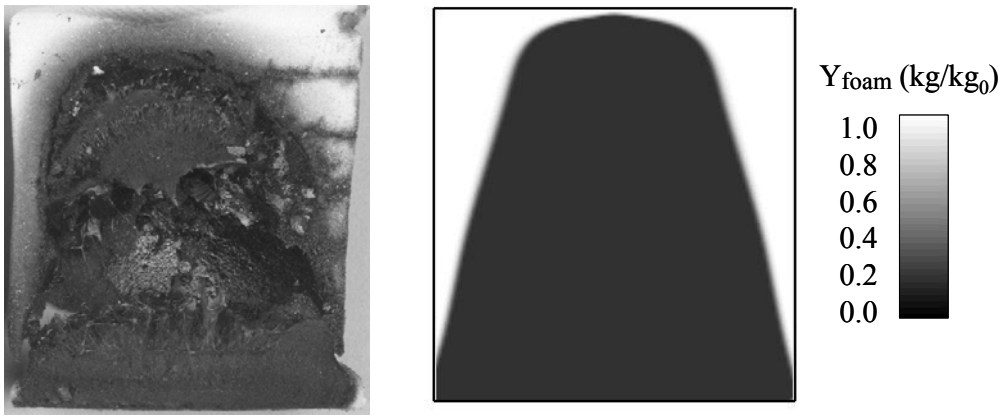

(a) **(b)**

Fig. 3. Qualitative comparison of model and experimental data.

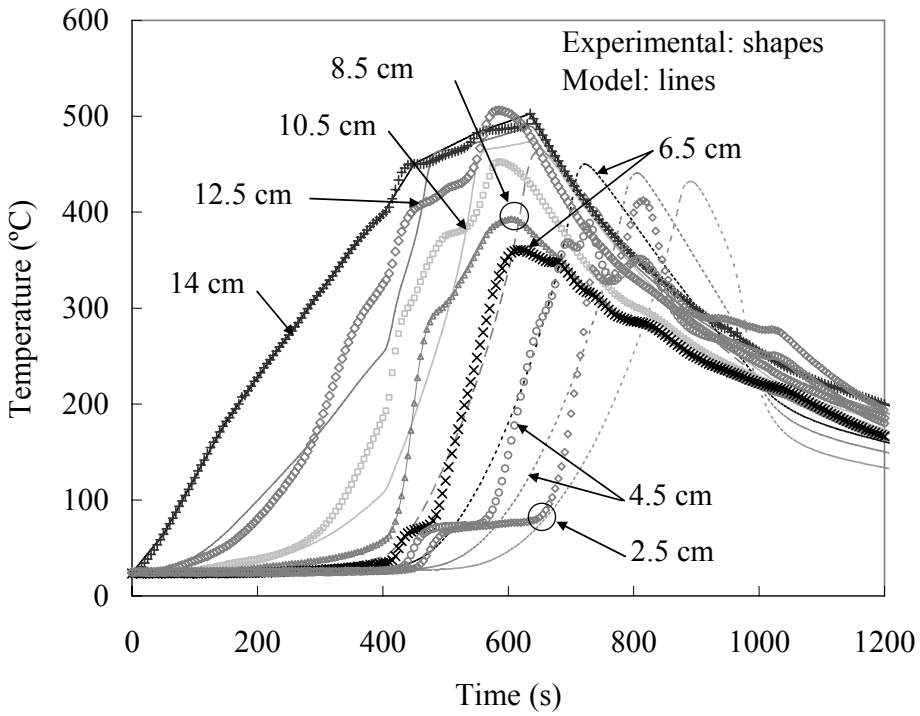

Fig. 4. Two-dimensional model vs. experimental comparison at seven centerline thermocouple locations (solid lines: model data, shapes: experimental data).

List of Figures: